Photoinduced Aggregation of Polymer Nanoparticles in a Dilute Nonaqueous Dispersion

Chunlin Zhou,[†] Yue Zhao,[‡] Tze-Chi Jao,[||] Mitchell A. Winnik,*[,†] and Chi Wu*[,‡,§]

Department of Chemistry, University of Toronto, Toronto, Canada, M5S 3H6, The Open Laboratory of Bond-selective Chemistry, Department of Chemical Physics, The University of Science & Technology of China, Hefei, Anhui 230026, China, Department of Chemistry, The Chinese University of Hong Kong, Shatin, N.T. Hong Kong, and Ethyl Petroleum Additives, Inc., 500 Spring St., Richmond, Virginia 23218-2189

Received: September 12, 2001; In Final Form: November 28, 2001

We describe the photoinduced flocculation of a nonaqueous dispersion of core−shell nanoparticles (diameter = 50 nm). The particles consist of a tightly cross-linked core composed of poly(butyl methacrylate-*co*-ethylene glycol dimethacrylate) and a lightly cross-linked shell of poly(butyl methacrylate-*co*-ethylene glycol dimethacrylate-*co*-methacrylic acid). After converting the acid groups in the shell to 1-phenylketo-2-octadecyl ester groups, the particles could be dispersed in cyclohexane, sterically stabilized by the alkyl substituents of these ester groups. Photocleavage of these substituents ($\lambda = 310$ nm) regenerated the −COOH groups and led to slow aggregation of the destabilized particles. This system allowed us to study the process of particle aggregation kinetics in the absence of long-range electrostatic interaction by using a combination of static and dynamic laser light scattering. Our results show that there exist two stages in the aggregation process. Initially, several particles come into contact to form small, elongated clusters. Subsequently, these clusters undergo further aggregation to form larger aggregates characterized by a fractal dimension of 2.3. Our results indicate that aggregation in the second stage follows a reaction-limited cluster−cluster aggregation mechanism. We also found that the average radius of gyration $<R_g>$ during aggregation scaled with time with an exponent of 1.4 ± 0.1, much higher than predicted and found in previous experiments.

Introduction

The aggregation of polymeric particles is an important phenomenon in physics, chemistry, biology, medicine, and engineering. Both theoretical[1−5] and experimental[6−11] studies have been undertaken in this area, with a particular focus on the aggregation kinetics and the structures of resultant aggregates. It is generally accepted that there exist two limiting regimes for aggregation: diffusion-limited cluster−cluster aggregation (DLCA) and reaction-limited cluster−cluster aggregation (RLCA).[1,2,12−15] The regime to which an actual aggregation process belongs is determined by the sticking probability between particles or clusters when they collide. In DLCA, the sticking probability of each encounter is close to 100%. The aggregation rate is controlled by the average time taken for two clusters to collide. On the other hand, RLCA refers to the process in which the sticking probability is so low that many collisions occur before particles and clusters combine into larger aggregates.

One of the distinctive features that distinguish DLCA and RLCA is the geometry of the aggregates that form. DLCA and RLCA differ in the fractal dimensions (d_f) of the resultant aggregates,[2,16] where the fractal dimension refers to the scaling between the mass (M) and size (R) of the aggregates, $M \sim R^{df}$. The DLCA process leads to aggregates with an open and less uniform structure, with $d_f \sim 1.7-1.8$ for a three-dimensional system. The kinetics of DLCA is characterized by a scaling between the size and the aggregation time (t), $R \sim t^{\alpha}$ with $\alpha <$ 1. In contrast, the RLCA process leads to more uniform aggregates with a higher fractal dimension in the range 2.0−2.5, because an approaching particle has a higher chance to penetrate into the "fjords" of a cluster before it sticks to the cluster.[3,17−19]

The RLCA process is often observed for hyperbranching polymerizations[20−23] and for some ionic-strength-induced aggregation in the presence of a low content of salt. In this aggregation process, when the salt concentration is low, a substantial, but not in surmountable, repulsive force exists between two clusters (particles).[8,9] The aggregation rate in this case is limited by the time taken for the aggregating species to overcome this repulsive barrier by thermal activation. Ball et al.[24] pointed out that in a real experiment the polydispersity of the resultant clusters could result in a slightly higher value of d_f than that predicted theoretically. Weitz et al.[15] suggested that in the RLCA process, R should increase exponentially with time as $R \sim \exp(At)$, where A is a constant, whose value depends on the system studied.

In comparison with aqueous dispersions, the study of the aggregation of colloidal particles in nonaqueous media is rather limited.[25] Nonaqueous colloidal particles in nonpolar media are often stabilized by chains attached to surface that would be soluble in the medium if they were free of the surface. Because this corona is "swollen" by the medium, the interaction between the coronas on approaching particles provides a strong repulsive force between them. Two factors contribute to this repulsion. One is osmotic, related to the tendency of solvent to diffuse into the domains of overlapping coronas, where the solute concentration is temporarily elevated. The other is entropic, since corona overlap lowers the configurational entropy of the stabilizer chains. One can induce the aggregation of a nonaqueous dispersion by decreasing the solvency of the medium for

* To whom correspondence should be addressed.
[†] University of Toronto.
[‡] The University of Science & Technology of China.
[§] The Chinese University of Hong Kong.
[||] Ethyl Petroleum Additives, Inc.

10.1021/jp013498f CCC: $22.00
Published on Web 02/02/2002

SCHEME 1

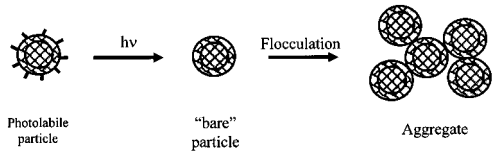

the attached chains, either by changing the temperature or by adding a poor solvent to the solution.

Alternatively, one could use a photochemical reaction to induce flocculation. For example, one could introduce a photoisomerable group into the stabilizer chains in such a way that the photoreaction decreased the solvency of the medium for the particles.[26] Here we take a more drastic approach. The particles we examine have the stabilizer chains attached by a photolabile group. Irradiation of the particles cleaves the stabilizer chains from the particles and leaves in their place a much more polar group. An overview of this process is shown in Scheme 1. In a previous publication,[27] we described the synthesis of tiny core−shell particles that meet the needs of this type of experiment. These particles, with a mean diameter (dry) of 50 nm, have a narrow size distribution and can be dispersed in aliphatic hydrocarbon solvents. The $-C_{16}H_{33}$ chains in the stabilizer are attached to the particle surface by an α-benzoyl ester group. Upon irradiation with UV light (λ = 310 nm), this group fragments, leaving in its place the −COOH group. Flocculation is driven by the absence of stabilization and by the tendency of the −COOH groups to dimerize. The experiments reported here were carried out in cyclohexane, in which the photolabile particles form a stable colloidal dispersion. Upon irradiation, flocculation begins, but in cyclohexane this process is very slow and provides adequate time to carry out dynamic (DLS) and static laser light scattering (SLS) measurements as the aggregation process proceeds. SLS provides a direct method to evaluate the fractal dimension d_f of the aggregates, because both the molar mass and size of the resultant aggregates can be measured directly. In addition, the asymptotic behavior of the scattered intensity $I(q)$ is given by $I(q) \propto q^{-df}$ when $R_{aggregate} > q^{-1} > R_{particle}$, where q is the scattering vector.

One of the motivating factors of this work is to try to model the flocculation−precipitation process that leads to sludge formation inside a hot automobile engine or soot agglomeration in a diesel truck engine. In contemporary technology, dispersing agents (soluble polymers with different chain ends or lengths) are added into motor oil to trap and stabilize tiny particles formed in the oil. The effectiveness of a given dispersing agent is normally assessed by a macroscopic time-consuming trial-and-error procedure. Improving this technology requires a better understanding of the aggregation process. For example, Bezot et al.[25a] recently described aggregation experiments on soot particles taken directly from diesel engine tests. The authors sonicated the soot particles in clarified base oil and then studied their aggregation by a combination of dynamic and static light scattering. From the fractal nature of the growing aggregates and the magnitude of the fractal exponent (2.15 ± 0.1), they concluded that these soot particles grow by an RLCA process. Here we take the view that this kind of aggregate growth process can be better understood through the study of model systems in which one knows the structure of the aggregating particles and can control the onset of the aggregation process. Model studies not only help one to understand the mechanism of the aggregation process in hydrocarbon media, they also provide a mechanistically-based method[25b] to assess the effectiveness of different dispersing agents.

Experimental Section

Materials. *n*-Butyl methacrylate (BMA, Aldrich), ethylene glycol dimethacrylate (EGDMA, Aldrich), methacrylic acid (MAA, Aldrich), and 2-hydroxyethyl methacrylate (HEMA, Aldrich) were vacuum distilled under N_2 atmosphere and stored in the refrigerator before use. Sodium dodecyl sulfate (SDS, Aldrich), potassium persulfate (KPS, Aldrich), sodium bicarbonate (SBC, Fisher), cesium carbonate (Cs_2CO_3, Aldrich), cyclohexane (C_6H_{12}, BDH Laboratory Supplies), and other solvents were used as received. Water was purified by a Millipore Milli Q purification system.

Sample Preparation. The photolabile core−shell nanoparticles were prepared by a three-step procedure, described in more detail in ref 27. In the first step, the core (diameter ca. 20 nm) was prepared from a 4:3 mole ratio of BMA and EGDMA (with two methacrylate groups per molecule) by batch emulsion polymerization at 80 °C. In the second step, a monomer solution composed of 10 mol % MAA, 3 mol % HEMA, 4 mol % EGDMA, and 83 mol % BMA was fed continuously into a dispersion of these cross-linked first-stage seed particles under monomer-starved conditions to create a shell (13.5 nm thick) containing −OH and −COOH functional groups. After the reaction, the surfactant and other water-soluble ionic materials were removed from the dispersion by ion exchange (Bio-Rad beads, AG-501-X8) at room temperature. This process was repeated until no sodium ions were detected by a flame test. The ion-exchange resin beads themselves were removed by gravity filtration. The cleaned latex dispersion was neutralized to pH = 9.3 with a solution of Cs_2CO_3 and freeze dried.

In the final step, the freeze-dried particles (2.0 g) were suspended in *N*,*N*-dimethyl formamide (DMF, 20 mL). Under stirring, 1-phenyl-2-bromooctadecanone (0.6 g) was added at room temperature, and the reaction was allowed to proceed for 3 days. To remove the byproduct CsBr, ion-exchange resin beads were added to the reaction medium and the system was stirred for 24 h. The ion-exchange resin beads were separated by gravity filtration, and the process was continued until no Cs^+ ions could be detected by a flame test. Then the dispersion was concentrated on a rotary evaporator, and the resultant particles were precipitated with methanol. UV analysis indicated that 50% of the −COOH groups in the particles had been converted to 1-phenyl-1-oxo-2-octadecyl ester groups.

When dry, the resultant particles could be dispersed in cyclohexane. The cyclohexane dispersion was filtered into the light-scattering cell through a 45 μm Millipore filter to remove dust. The aggregation of these particles was induced in-situ inside the LLS cell by irradiation in a photochemical reactor for a few hours.

Photocleavage. The photocleavage reaction was carried out in a homemade photoreactor, whose design is shown Figure 1. The reactor consists of a box that holds eight 310 nm 15 W lamps (Gu Cun photoelectron factory, Shanghai, China) arranged in two layers on the inside wall of the reactor. Individual samples were suspended by a fine copper wire through the hole in the top of the reactor and positioned at the level of the bottom layer of lamps. The samples were irradiated directly in the Pyrex light-scattering cell (SUPERLCO 7.4 mL vial, Cat. No. 27150-U). While this combination of sample cell and irradiation system was adequate for the experiments described here, because the flocculation process was so slow, it has its shortcomings. The photoreaction was much less efficient than the corresponding reaction carried out in Toronto using a Rayonet photochemical reactor equipped with 12 RPR 310 nm lamps (Southern New England Ultraviolet Co.).[27] Under those conditions, the photo-

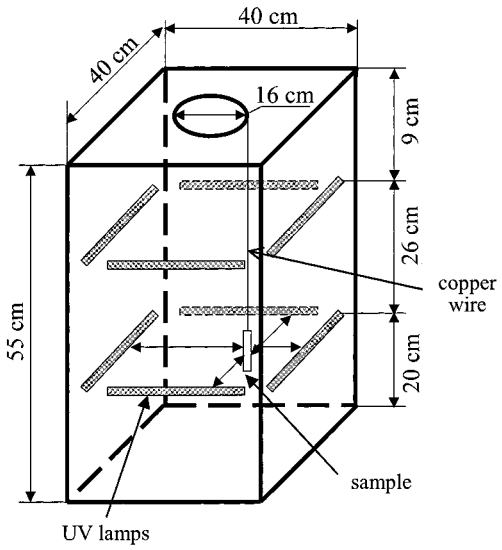

Figure 1. Drawing of the photoreactor with eight 15 W UV lamps.

reaction was essentially complete in 7 min. Part of the problem is caused by irradiation through the Pyrex cell, which absorbs about 60% of the incident light at 310 nm.

Laser Light Scattering. Light scattering measurements were carried out with a modified commercial light scattering instrument (ALV GmbH, Langen, Germany), equipped with a multi-tau digital time correlator (ALV-5000) and a solid-state laser (ADLAS DPY 425II, output power ca. 400 mW at $\lambda = 532$ nm). The details of this instrument can be found elsewhere.[28] In static light scattering, the angular dependence of the absolute excess time-averaged scattered intensity, the Rayleigh ratio $R_{vv}(q)$, is related to the weight-average molar mass (M_w), the z-average root-mean-squared radius of gyration ($\langle R_g^2\rangle_z^{1/2} \equiv \langle R_g\rangle$) of the scattering objects, and the second virial coefficient (A_2) of the dispersion by

$$\frac{Kc}{R_{vv}(q)} \cong \frac{1}{M_w}\left(1 + \frac{1}{3}\langle R_g^2\rangle_z q^2\right) + 2A_2c \qquad (1)$$

where K is a constant for a given dispersion, temperature, and laser and q [$= (4\pi n/\lambda)\sin(\theta/2)$] is the scattering vector with n, λ, and θ being the refractive index of solvent, the wavelength of the light in a vacuum, and the scattering angle, respectively. For a fractal object formed by aggregation of colloidal particles, the scattered intensity $I(q)$ scales with q as $I(q) \sim q^{-df}$ in the range of $R_{aggregate} > q^{-1} > R_{particle}$, where d_f is the fractal dimension. $R_{particle}$ and $R_{aggregate}$ are the radii of the primary particles and the resultant aggregates, respectively.[29] When $q^{-1} < R_{particle}$, the light probes the internal structures of the primary particles and the intensity profile reflects the density distribution inside, whereas when $q^{-1} > R_{aggregate}$, the average size of the resultant aggregates and the correlation of the topological length between the aggregates could be determined.

In this research, the size of the aggregates grows from 40 nm to approximately 500 nm. To analyze the data for this wide range of aggregate sizes, we use the Zimm method[30] to calculate $\langle R_g\rangle$ and M_w when the rms radius of gyration $\langle R_g\rangle$ is less than 100 nm. We employed the Berry method[31] when $\langle R_g\rangle$ is larger than 100 nm.

In dynamic light scattering (DLS), the cumulant analysis of the measured intensity−intensity time correlation function $G^{(2)}(q,t)$ in the self-beating mode provides an average line-width ($\langle\Gamma\rangle$), and Laplace inversion analysis provides the line-width distribution ($G(\Gamma)$).[32,33] For a pure diffusive relaxation, Γ can be related to the translational diffusion coefficient D via $\Gamma = Dq^2$ in the limit of $c \rightarrow 0$ and $q \rightarrow 0$,[34] where c is the concentration of scatters. The hydrodynamic radius (R_h) can be calculated by the Stokes−Einstein equation

$$D = k_BT/(6\pi\eta R_h) \qquad (2)$$

where k_B is the Boltzmann constant, T is the absolute temperature, and η is the solvent viscosity. Therefore, $G(\Gamma)$ can be converted to a hydrodynamic radius distribution $f(R_h)$: From each line width distribution $G(\Gamma)$ or hydrodynamic radius distribution $f(R_h)$, we calculate an average line width ($\langle\Gamma\rangle$, defined as $\int_0^\infty G(\Gamma)\Gamma\, d\Gamma$) or an average hydrodynamic radius ($\langle R_h\rangle$, defined as $\int_0^\infty f(R_h)R_h\, dR_h$) characteristic of the sample.

SCHEME 2

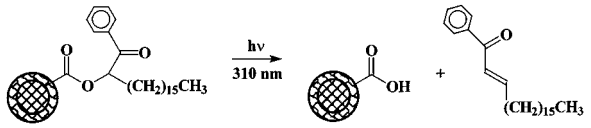

Results and Discussion

Structure and Stability of the Photolabile Particles. The structures of the surface groups on the particles we examine, and the products of their photoreaction, are shown in Scheme 2. These particles were synthesized in aqueous solution, modified in DMF, purified, and then dried. In these particles, half of the carboxylic acid groups in the shell were converted to α-benzoyl heptadecyl ester group. The dry powder could be easily dispersed in various aliphatic hydrocarbon solvents, such as cyclohexane and cyclohexane−hexadecane mixtures. The particles did not form stable colloidal dispersions in pure hexadecane, a result that suggests that the relatively short stabilizer chains do not provide sufficient steric stabilization in this solvent. In contrast, these photolabile particles form very stable dispersions in cyclohexane. The dispersion could be filtered through a submicron filter, and no flocculation could be detected when these dispersions were stored in the dark for periods of up to 10 months. Under these circumstances, the energy barrier due to osmotic and entropic repulsion of the stabilizer chains is sufficient to overcome the relatively weak van der Waals attraction between the particles. Since the particles are uncharged and in a low dielectric medium, there is no significant electrostatic repulsion between the particles. Upon irradiation at 310 nm, a photocleavage reaction removes the stabilizer chains and replaces nonpolar ester groups with −COOH groups. Under the conditions employed here (see the Experimental section), this reaction is rather slow and requires several hours to go to completion. The C_{16} chain contribution to steric stabilization is removed and replaced with attractive hydrogen bonding interactions between pairs of the newly created −COOH groups and between these −COOH groups and the −OH originally in the shell of the particles. The barrier to flocculation is reduced significantly, and aggregation begins.

Figure 2 shows that the process that we observe upon photocleavage of the benzoyl ester groups is more subtle than simply cutting the stabilizing hairs from the surface of a hard sphere. In Figure 2 we plot values of the average hydrodynamic radius $\langle R_h\rangle$ and the average radius of gyration $\langle R_g\rangle$ of the particles in cyclohexane as the photochemical reaction proceeds. We find that both values decrease with increasing irradiation time and level off after about 3.5 h. Under these conditions, the ratio of $\langle R_g\rangle/\langle R_h\rangle$ remains constant and close to the

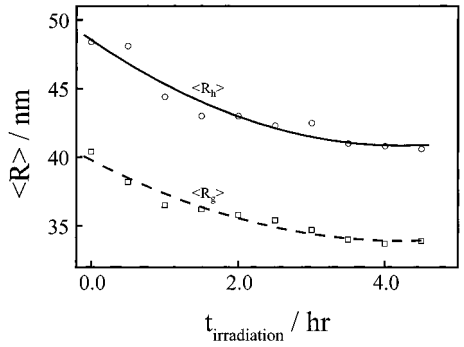

Figure 2. Irradiation-time-dependence of the average size ($<R_g>$, $<R_h>$) of PBMA core−shell nanoparticles. UV light ($\lambda = 310$ nm) was used to cleave the stabilizing α-benzoyl heptadecyl chains.

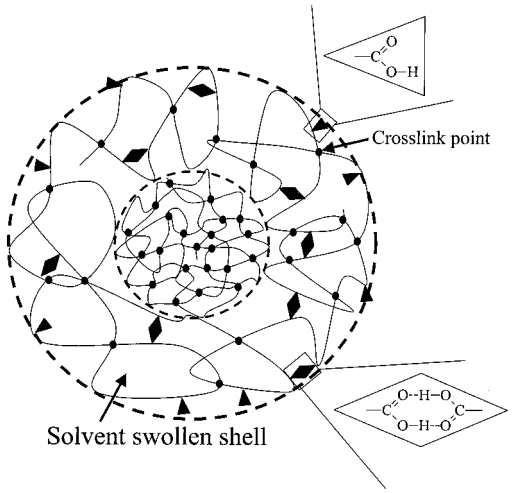

Figure 3. Schematic drawing of the structure of the swollen nanoparticles in cyclohexane.

theoretical value of 0.78 predicted for a uniform sphere, indicating that the particles are spherical and do not aggregate on this time scale. It is important to note that the C_{16} chains have a fully stretched length of only ca. 2 nm, whereas both $<R_h>$ and $<R_g>$ decrease by about 7 nm. This result can be understood by recognizing that the dry thickness of the particle shell that contains the ester groups is approximately 13 nm thick. Removal of the ester groups and their conversion into −COOH groups will decrease the quality of the solvent for the polymer in this shell. In other words, we expect the photoreaction to increase the magnitude of the Flory−Huggins χ parameter for the shell polymer in cyclohexane, accompanied by a deswelling of this shell. This deswelling by solvent is the cause of the decrease in particle radius seen in Figure 2.

The diameter of the dry particles prior to irradiation is about 50 nm, nearly the same size as their precursor latex particles synthesized in water. Scheme 3 shows that the diameter of these particles increases to about 95 nm when these particles are dispersed in cyclohexane due to the swelling of the particles themselves in this solvent. When the shell layer of the particles was modified by the photoreaction, the particle diameter decreased to about 80 nm. This value is still significantly larger than the 50 nm radius of the dry particles, indicating that even after the photoreaction and before the onset of aggregation, cyclohexane is still able to induce swelling of the particles. Figure 3 shows a schematic representation of the shell-swollen core−shell nanoparticle after irradiation. Most of the acid groups are dimerized in the shell. In Table 1, we list the average number of monomer units ($<N^c>$) and the average molecule weight ($<M^c>$) between cross-link points for these particles. Assuming

SCHEME 3

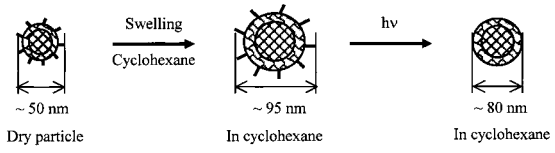

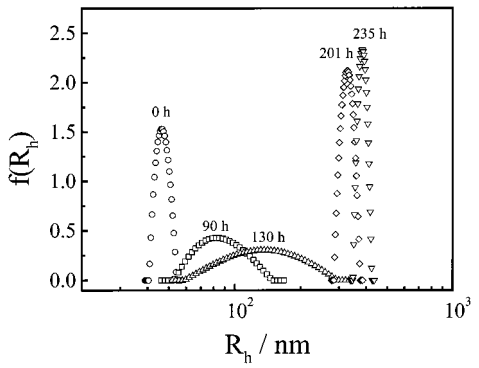

Figure 4. Time dependence of the hydrodynamic radius distribution ($<R_h>$) of the aggregates after 4.5 h irradiation of the precursor particles.

TABLE 1: Average Number of Monomer Units and Molar Mass and Number of Functional Groups between the Cross-link Points in the Core and Shell

	$<N^c_{BMA}>$	$<M^c_{BMA}>$	$<N^c_{MAA}>$	$<N^c_{HEMA}>$
core	1.33	189	−	−
shell	20.7	2950	2.50	0.75

complete conversion of polymerizable group of EGDMA, there are fewer than two monomer units between cross-links in the core, whereas there are more than twenty in the shell. For the functional group −COOH in the shell, there are 2 to 3 units between cross-link points. Compared with the highly cross-linked core, the shell is relatively loose and easily swollen by a good solvent.

At longer times, the particles aggregate, and the increase in aggregate size can be monitored by light scattering. In Figure 4 we plot the change in hydrodynamic radius distribution $f(R_h)$ obtained from Laplace inversion of the dynamic light scattering signal, against R_h, for different times after photoirradiation of the sample. One sees first that the time scale for the particle growth process is much longer, tens of hours to 10 days, than the time for the photoreaction to take place. The plot at zero time shows that the original particles have a narrow size distribution. In the initial stages of aggregation, the size distribution broadens, and the peak is shifted to a larger radius. Later stages of aggregation lead to larger aggregates, but with a much narrower size distribution.

Aggregation is sufficiently slow that we can measure the angular dependence of the integrated (static) light scattering intensity as a function of aggregation time. These are the data needed to calculate the weight-averaged molecular weight of the aggregates as a function of time, as well as their radius of gyration. In analyzing these data, we employ a Zimm analysis[30] to calculate the *z*-averaged root-mean-squared radius of gyration, $\langle R_g^2\rangle_z^{1/2}$, for samples that yield values of R_g less than 100 nm. For larger aggregates, we employ a Berry analysis.[31] Both treatments yield similar values of R_g in the small particle regime, as shown in Figure 5. For larger aggregates, the results of the two analyses diverge.

In Figure 6 we examine the influence of irradiation time on the rate of growth of the aggregates. In this figure, we plot the log of the mean hydrodynamic radius $<R_h>$ against aggregation

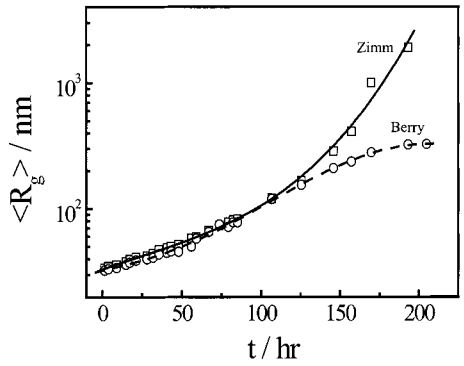

Figure 5. Time dependence of *z*-average root-mean-squared radius of gyration (<R_g>) of the aggregates, calculated by the Zimm and Berry methods, respectively.

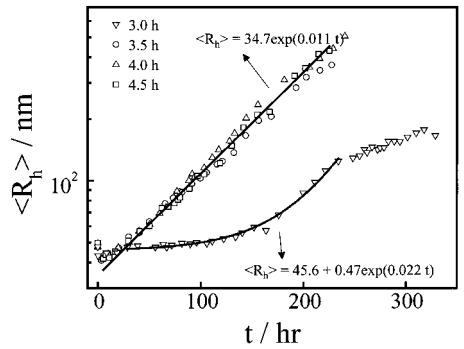

Figure 6. Time dependence of the average hydrodynamic radius (<R_h>) for samples subjected to different irradiation times. The line represents a least-squares fitting of <R_h> (nm) = 34.7 exp(0.011*t*) for $t_{irradiation}$ > 3.5 h.

time *t*. For irradiation times (t_{ir}) greater than 3.5 h, we find that all the data fall on a common line, which exhibits an exponential dependence of <R_h> on aggregation time, which can be fitted to the expression

$$<R_h> = 34.7 \exp(0.011\, t) \tag{3}$$

As shown in Figure 2, the values of <R_h> after 3.0 h irradiation are slightly higher than those after 3.5 h irradiation, indicating that the photoreaction is not complete, and that a small fraction of the long alkyl chains remain on the particle surface. Figure 6 clearly shows that this small number of the remaining chains can significantly reduce the sticking probability and slow the aggregation. This kind of slow-down in aggregation kinetics was also observed in the salt-induced aggregation of latex particles in aqueous solution in the presence of absorptive polymer chains.[35,36] It illustrates that in practice only a small number of soluble chains attached to the particle surface can be sufficient to stabilize the dispersion against aggregation. Figure 6 also emphasizes the slow rate of the aggregation process and suggests that, with the reactor and sample vials used in these experiments, 3.5 h irradiation was sufficient to cleave all of the stabilizer chains attached to the particles. It also suggests that the aggregation followed the RLCA mechanism.

Kinetics of Photoinduced Aggregation. The slow rate of the aggregation process is strongly suggestive of a reaction-limited cluster aggregation process. One of the ways to lend support to this conclusion is to estimate the time necessary for aggregation in a diffusion-limited process. If Brownian flocculation is fast and diffusion controlled, as described by Smoluchowski, and sedimentation flocculation is assumed to be negligible, the diffusion-controlled rate constant is given by

$$k_{diff} = 8\pi N_A R_h D \tag{4}$$

where N_A is Avogadro's number and *D* is the particle diffusion coefficient. Equation 4 can be simplified by using the Stokes−Einstein eq 2 to yield

$$k_{diff} = 4RT/3\eta \tag{5}$$

where *R* (= $k_B N_A$) is the gas constant. The two-particle association rate for two identical particles is described by second-order kinetics

$$-\mathrm{d}c/\mathrm{d}t = k_{diff} c^2 \tag{6}$$

where *c* is the concentration of particles at time *t*. Integration of eq 6 yields the total concentration of doublets and single particles,[37,38]

$$c = c_o/(1 + t/T_{1/2}) \tag{7}$$

where $T_{1/2}$, the time at which *c* will be half of c_0, is given by

$$T_{1/2} = 1/k_{diff} c_o \tag{8}$$

In the case where further flocculation leads to triple and higher order droplets, the total concentration is also given by eq 7.

Where a repulsive barrier is present, the rate constant for slow flocculation is given by $k_{slow} = k_{fast}/W$, where *W* is the stability ratio and k_{fast} is the rate constant in the Smoluchowski limit. The stability ratio is defined theoretically in terms of the interparticle potential Φ as

$$W = 2\mathrm{R}\int_{2R}^{\infty} \exp\left(\frac{\Phi}{k_B T}\right) r^{-2}\, \mathrm{d}r \tag{9}$$

The potential has been calculated for spherical particles with anchored chains using lattice fluid self-consistent field theory.[39]

The experiments reported here were carried out at a particle concentration of 0.23 mg/mL, corresponding to 1.4×10^{-9} mol/L particle concentration (8.4×10^{14} L^{-1}).[40] To calculate the particle concentration, we use the radius of the dry particles and take the dry polymer density to be 1.05, since its main component is poly(butyl methacrylate). From the measured values of *D* and R_h we calculate a value of $k_{diff} = 3.7 \times 10^9$ L mol^{-1} s^{-1}. Thus the initial rate of the particle dimerization is estimated to be 6.8×10^{-9} mol L^{-1} s^{-1}, and the primary particles will collide and stick together to form dimers in less than a second. Subsequent steps in the DLCA process will be slower as the number density of clusters decreases, but diffusion-limited aggregation would be expected to take place on a time scale of seconds. In our experimental results, aggregation occurs on a time scale that is many orders of magnitude longer. We infer that only a small fraction of collisions are sticky, and that aggregation occurs by the RLCA process.

Lin et al.[41] comment that RCLA aggregation kinetics are best described as an exponential, $M \sim \exp(At)$. We plot our results in Figure 7. While we can fit all data points to a single line [$M_w = (6.86 \pm 0.06) \times 10^7 \exp\{(0.0082 \pm 0.0008)t\}$], we provide evidence below that there are two stages to the cluster growth process. In the second stage $M_w = (6.69 \pm 0.06) \times 10^7 \exp\{(0.0096 \pm 0.0005)t\}$.

The slow rate of particle aggregation implies that two colliding particles or two colliding clusters have an activation barrier to overcome in order for the two species in contact to

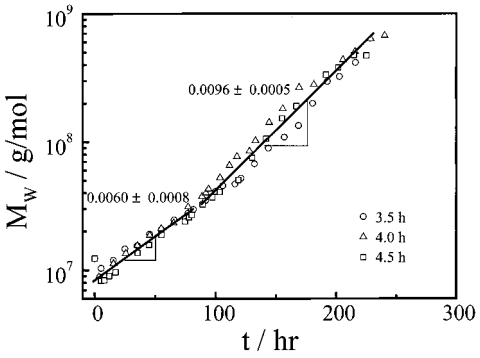

Figure 7. A plot of log M_w against time for aggregation of samples subjected to different irradiation times. There are two stages to the aggregation process. For $t < 100$ h, $M_w = (6.94 \pm 0.06) \times 10^7$ exp-$\{(0.0060 \pm 0.0008)t\}$. For $t > 100$ h, $M_w = (6.69 \pm 0.06) \times 10^7$ exp-$\{(0.0096 \pm 0.0005)t\}$.

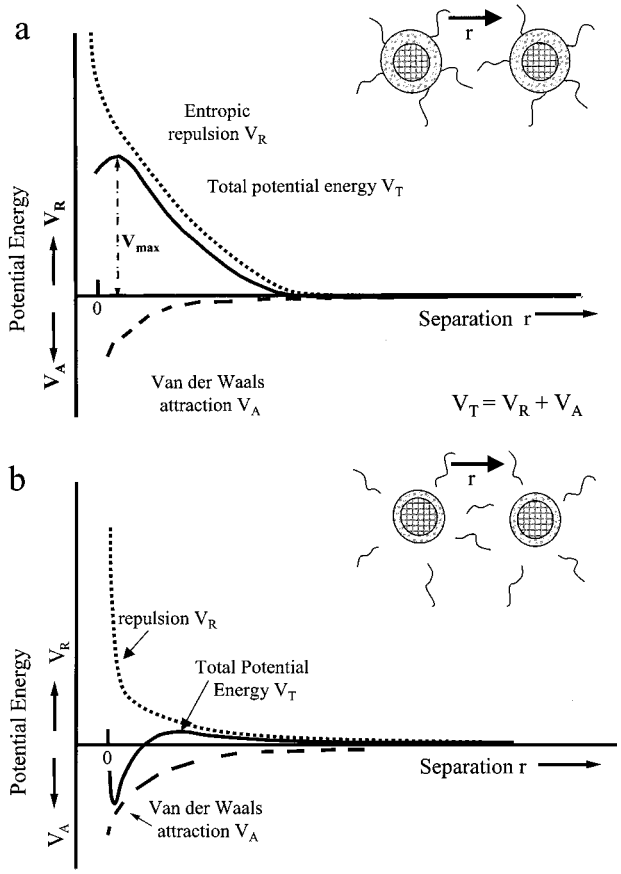

Figure 8. A potential energy diagram for the interaction of pairs of nanoparticles: (a) with steric stabilizer chains (before irradiation); (b) without stabilizer chains (after irradiation).

stick. We depict the energetics of particle interaction in Figure 8, where in Figure 8a we present an energy diagram of the system prior to the photoreaction, and in Figure 8b, the corresponding energy diagram after UV irradiation. In the as-prepared dispersion, the entropic repulsive energy and the osmotic interaction between particles are associated with solvent swelling of the shell layer. They provide a barrier that is much larger in magnitude than the relatively weak van der Waals attraction. One of the reasons that the van der Waals attraction is so weak is that the particles are swollen by the solvent. After photocleavage of the nonpolar ester groups, the composition of the shell polymer changes. The −COOH groups introduced into the shell decrease the extent to which cyclohexane can swell this polymer. This reaction has two consequences on the particle−particle interaction. First, the decrease in solvency decreases the magnitude of the repulsive interaction. In addition, the decrease in swelling increases the magnitude of the van der Waals attraction.

The potential energy of interaction between two particles is normally treated in terms of a Lennard-Jones potential, assuming that the total free energy of interaction is obtained by summing the contributions from all possible pairs of molecules.[42] When the particles are close ($H/R \ll 1$),

$$\Delta G^{att} = -(A_H R/12H)[1 + (3/4)H/R + ...] \qquad (10)$$

where R is the radius of the particles, H the distance between the particles, and A_H the Hamaker constant. Generally, it is sufficient to neglect all but the first term in the square brackets

$$A_H = (3/4)h\nu\alpha^2 n_v^2 \qquad (11)$$

where h is Planck's constant, ν is a characteristic frequency identified with that corresponding to the first ionization potential, α is the polarizability of the atom or molecule, and n_v is the number of molecules per unit volume of particles. For us, the important feature of eq 11 is that the Hamaker constant A_H depends on the difference in polarizability between the particles and the medium, and that this difference changes when the particles are swollen by the solvent.

$$\Delta A_H \propto \alpha^2_{polymer} - \alpha^2_{solvent} \qquad (12)$$

When the shell is swollen by the cyclohexane, the difference in polarity between the particle and the medium is reduced because of the presence of the solvent inside the particle. The Hamaker constant is reduced in value, and the sticking probability becomes smaller when two particles collide. Our results are in accord with this view.

Aggregation begins by a process that requires overcoming an activation energy. This activation energy is unlikely to be due to an electrostatic repulsion between ionized −COOH groups in a low dielectric medium like cyclohexane. Rather, we imagine that the limited extent of swelling of the particles by the solvent provides a steric barrier to aggregation. Other observations to be reported separately[43] support this idea. For example, when the photolabile particles are irradiated in mixtures of cyclohexane and hexadecane, the aggregation rate increases significantly with the hexadecane content of the medium. Hexadecane is such a poor solvent for the PBMA copolymer that the particles before irradiation do not form stable dispersion in this solvent. We infer that decreased swelling of the particles leads to an increased attractive interaction and a decreased repulsion between the particles.

Two Stages of Aggregation. In Figure 9 we saw that the initial stages of aggregation led to the formation of clusters with a broad size distribution, and that at later stages the larger aggregates formed had a much narrower size distribution. This result suggests that aggregation occurs in two stages with very different properties. The variation of the size distribution as a function of time can be better viewed by examining the relative width of the distribution [$(\mu_2/<\Gamma>^2)$ of $G(\Gamma)$], where μ_2 is defined as $\int_0^\infty G(\Gamma)(\Gamma - <\Gamma>)^2\, d\Gamma$. We show the plot of $\mu_2/<\Gamma>^2$ vs time in Figure 9. Despite the scatter in the data points, the trend is clear. The width of the distribution grows over the first 100 h after the photoreaction and then decreases with increasing time.

In Figure 10 we plot the measured values of the average number of primary particles (M_w/M_0) in the aggregates as a

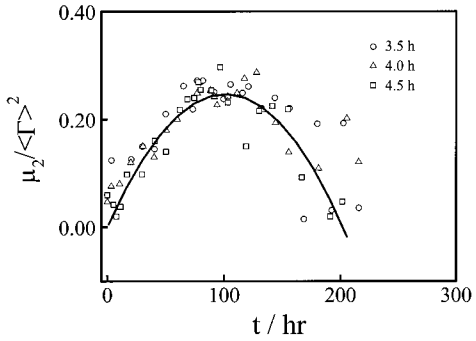

Figure 9. Time dependence of the relative width ($\mu_2/<\Gamma>^2$) of the line-width distribution ($G(\Gamma)$) for samples subjected to different irradiation times, where the particle concentration is 2.3×10^{-4} g/mL, $\mu_2 = \int_0^\infty G(\Gamma)(\Gamma - <\Gamma>)^2\, d\Gamma$and $<\Gamma> = \int_0^\infty G(\Gamma)\, \Gamma\, d\Gamma$.

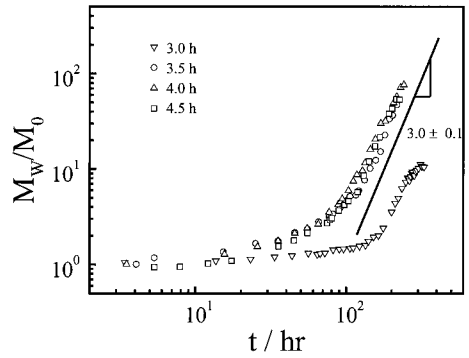

Figure 10. Time dependence of the average number of particles (M_w/M_0) formed through aggregation for samples subjected to different irradiation times. Static light scattering measurements at the end of the photoirradiation step yield $M_o = (8.6 \pm 0.2) \times 10^6$.

function of time. The weight averaged molecular weight of the primary particles (M_0) is $(8.6 \pm 0.2) \times 10^6$ g/mol. Here we also see two distinct stages in the aggregation process. In the first stage, M_w/M_0 increases slowly with time, crossing over to a second stage of aggregation in which M_w/M_0 increases much more rapidly with time. In the first stage, which can be thought of as an induction period lasting up to nearly 100 h, individual particles collide and stick to form small clusters. This induction period was longer for the particle dispersion irradiated for only 3 h, where the photochemical cleavage reaction is incomplete. In the second stage, the small clusters combine to form large aggregates. Despite the large difference in the length of the induction period for the samples irradiated for 3 h and for more than 3.5 h, the scaling between M_w/M_0 and t in the second stage is similar, namely, $M_w/M_0 \sim t^{3.0 \pm 0.1}$. It is known that for a DLCA process, $M_w \sim R^{df}$ and $R \sim t^{1/df}$, so that $M_w/M_0 \sim t$. Our observations are inconsistent with a DLCA process. We are unaware of a theoretical prediction of such a large scaling exponent for an RLCA process.

In Figure 11 we plot the increase in M_w against the corresponding increase in the average radius of gyration $<R_g>$. These data also show two stages in the aggregation process, with a crossover occurring at $<R_g> \approx 120$ nm. In the first stage, $M_w \sim <R_g>^{1.2 \pm 0.1}$, showing that each aggregate, on average, contains only a few particles. Assuming that these particles stick in a linear fashion like a series of pearls, we could calculate the values of $<R_g>$ of these small clusters, which are represented by the filled circles in Figure 11. It is clear that these theoretical values are parallel to the measured data and exhibit a similar scaling between M and R. Note that we did not consider size polydispersity in the calculation, which may explain why the measured $<R_g>$ is larger for a given molar

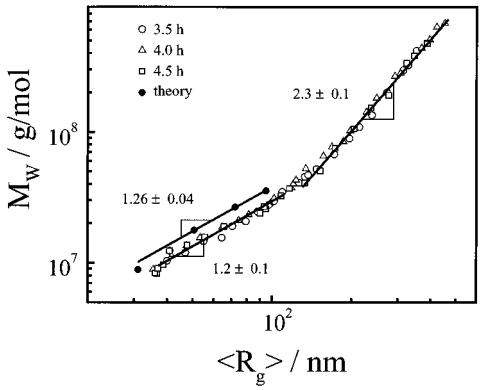

Figure 11. Scaling relationship between the weight-average molar mass (M_w) and the z-average radius of gyration ($<R_g>$), where the filled circles represent the results calculated for linear clusters consisting of two, three, and four particles.

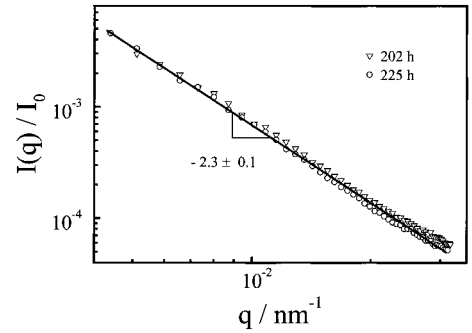

Figure 12. Scattering vector (q) dependence of the scattered light intensity of large aggregates ($q<R_g> > 1$) for samples subjected to different irradiation times.

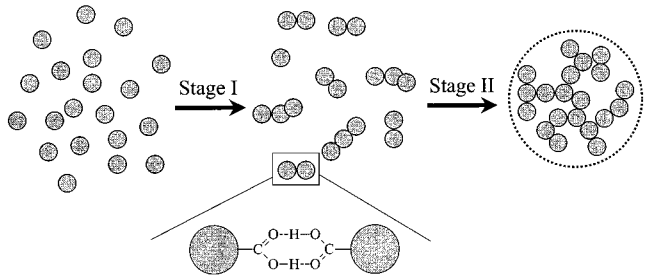

Figure 13. Representation of the two stages of aggregation after UV irradiation.

mass. In the second stage, the scaling exponent increases to 2.3 ± 0.1, a value characteristic of aggregates formed through an RLCA process. Further evidence for the fractal structure of these large aggregates is provided by the q-dependence of the scattering intensity. In Figure 12 we show that for aggregates with an average radius larger than q^{-1}, $I(q) \sim q^{-2.3}$. The magnitude of the scaling exponent is consistent with aggregates formed in a reaction-limited process.

We summarize our ideas about the two stages of the aggregation process in Figure 13. In the first stage, individual particles stick together to form a mixture of dimers, trimers, and other small clusters, leading to a large increase in the polydispersity of cluster sizes present in the sample. This is the polydispersity one sees in Figure 4 for the samples 90 and 130 h after the photoreaction. In the second stage, cluster−cluster aggregation becomes dominant, leading to the formation of large aggregates. The aggregation of these small clusters acts like an averaging process, so that the polydispersity decreases. This two-stage mechanism for particle aggregation predicts specific changes in the ratio of radius of gyration to hydrodynamic radius

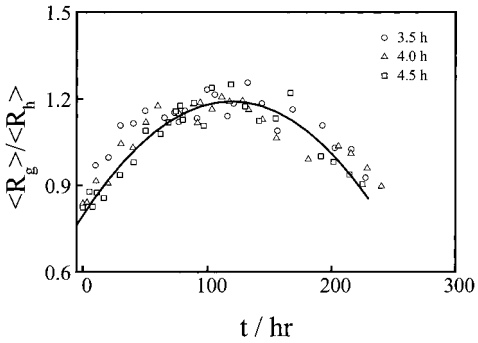

Figure 14. Time dependence of the ratio of the average radius of gyration to the hydrodynamic radius for samples subjected to different irradiation times.

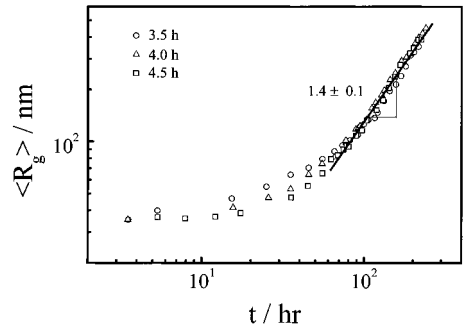

Figure 15. Time dependence of the radius of gyration ($<R_g>$) of the aggregates formed for samples subjected to different irradiation times.

($<R_g>/<R_h>$) as the aggregation proceeds. As one sees in Figure 14, the initial ratio is close to the value (0.78) predicted for uniform nondraining spheres. As the aggregation proceeds, this ratio increases, suggesting that the shape of the resultant clusters in the first stage is elongated. In the second stage, the aggregation of these elongated small clusters gradually leads to more compact sphere-like structures, so that $<R_g>/<R_h>$ decreases.

Conclusion

We used dynamic (DLS) and static (SLS) light scattering measurements to follow the time-course of the photoinduced aggregation of small polymer colloid particles dispersed in cyclohexane. The dried particles consist of a core composed of 20 nm diameter poly(butyl methacrylate-*co*-ethylene glycol dimethacrylate) with a relatively high cross-link density surrounded by a shell approximately 15 nm thick consisting of a lightly cross-linked PBMA copolymer containing functional groups. In the experiments reported here, the functional groups are C_{16} alkyl chains attached to the particle via photolabile α-benzoyl ester groups. The dried particles are easily dispersed in cyclohexane to form stable colloidal dispersions. Upon irradiation of the dispersion with 310 nm light, a photoreaction occurs, which cleaves the alkyl chains from the surface and transforms each of the esters to a polar $-$COOH group. The carboxyl-containing particles undergo slow aggregation in the cyclohexane medium.

The DLS experiments show that the individual particles are swollen by cyclohexane, increasing in diameter to 95 nm from about 50 nm in the dry state. Because the particle core has a relatively high cross-link density, we attribute this change in diameter primarily to solvent-induced swelling of the shell. After irradiation, the particle diameter decreases to 80 nm, indicating that the creation of $-$COOH groups in the shell polymer increases the χ value between this polymer and the solvent. This change in solvency creates a net attractive force between the particles, which is the driving force for the aggregation we observe.

Aggregation begins by a process that requires overcoming an activation energy. We explain the origin of this barrier by assuming that the limited extent of swelling of the particles by the solvent provides a steric barrier to aggregation. This point of view is supported by observations that when the photolabile particles are irradiated in mixtures of cyclohexane and hexadecane the aggregation rate increases significantly with the hexadecane content of the medium.

A combination of static and dynamic laser light-scattering studies showed that the aggregation process occurs in two stages. In the first stage, several particles come together to form a broad distribution of small elongated clusters, ranging from dimers and trimers to larger multiplets. In a second stage, these clusters undergo further aggregation into structures characterized by a fractal dimension of 2.3. Both stages of aggregation are governed by a reaction-limited cluster$-$cluster aggregation mechanism. One result that we are not able to explain is our finding that $<R_g>$ scales with time with an exponent of 1.4 ± 0.1, much higher than previously predicted and measured values (Figure 15).

In terms of our interest in modeling the formation of aggregates that lead to sludge formation in motor oil inside a hot running engine, we now recognize that the solvency of the hot oil for the polymeric material making up the particles themselves plays an important role in the aggregation process. If the "sludge-precursor" particles are dense and without stabilizing groups on their surface, they will likely aggregate in a diffusion-limited process. We note, however, that soot particles obtained from diesel engine oil have been found to undergo slow aggregation by an RLCA process.[25a] If the particles are subject to swelling by the oil medium, aggregation will be slower and will likely follow a reaction-limited mechanism.

Acknowledgment. The financial support of the RGC of HKSAR Earmarked Grant 1999/2000 (CUHK 426/00P, 2160135), the CAS Bai Ren Projector, Ethyl Petroleum Additives, Inc. and NSERC Canada is gratefully acknowledged.

References and Notes

(1) Witten, T. A., Jr.; Sander, L. M. *Phys. Rev. Lett.* **1981**, *47*, 1400.
(2) Meakin, P. *Phys. Rev. Lett.* **1983**, *51*, 1119.
(3) Brown, W. D.; Ball, R. C. *J. Phys. A* **1985**, *18*, L517.
(4) Martin, J. E.; Ackerson, B. J. *Phys. Rev. A* **1985**, *31*, 1180.
(5) Jullien, R.; Botet, R.; Mors, P. M. *Faraday Discuss. Chem. Soc.* **1987**, *83*, 125.
(6) Schaefer, D. W.; Martin, J. E.; Wiltzius, P.; Cannell, D. S. *Phys. Rev. Lett.* **1984**, *52*, 2371.
(7) Aubert, C.; Cannell, D. S. *Phys. Rev. Lett.* **1986**, *56*, 738.
(8) Lin, M. Y.; Lindsay, H. M.; Weitz, D. A.; Ball, R. C.; Klein, R.; Meakin, P. *Nature* **1989**, *339*, 360.
(9) Zhou, Z.; Chu, B. *J. Colloid Interface Sci.* **1991**, *143*, 356.
(10) Burns, J. L.; Yan, Y.; Jameson, G. J.; Biggs, S. *Langmuir* **1997**, *13*, 6413.
(11) Zhu, P. W.; Napper, D. H. *Phys. Rev. E*, **1994**, *50*, 1360; *Colloids Surf. A* **1995**, *98*, 93.
(12) Kolb, M.; Botet, R.; Jullien, R. *Phys. Rev. Lett.* **1983**, *51*, 1123.
(13) Jullien, R. J. *Phys. A* **1984**, *17*, L771.
(14) Von Schulthess, G. K.; Benedek, G. B.; De Blois, R. W. *Macromolecules* **1980**, *13*, 939.
(15) Weitz, D. A.; Huang J. S.; Lin, M. Y.; Sung, J. *Phys. Rev. Lett.* **1985**, *54*, 1416.
(16) Reinecke, H.; Mijangos, C.; Lopez, D.; Guenet, J. *Macromolecules* **2000**, *33*, 2049.
(17) Peng, S.; Wu, C. *Macromolecules* **1999**, *32*, 585.
(18) Vicsek, T. *Fractal Growth Phenomena*; World Scientific: London, 1992.

(19) Halsey, T. C. *Phys. Today* **2000**, *11*, 36.
(20) Chu, B.; Wu, C.; Wu, D. Q.; Phillips, J. *Macromolecules* **1987**, *20*, 2642.
(21) Chu, B.; Wu, C. *Macromolecules* **1988**, *21*, 1729.
(22) Wu, C.; Zuo, J.; Chu, B. *Macromolecules* **1989**, *22*, 838.
(23) Wu, C.; Chu, B.; Stell, G. *Makromol. Chem., Macromol. Symp.* **1991**, *45*, 75.
(24) Ball, R. C.; Weitz, D. A.; Written, T. A.; Leyvraz, F. *Phys. Rev. Lett.* **1987**, *58*, 274.
(25) (a) Bezot, P.; Hesse-Bezot, C.; Diraison, C. *Carbon* **1997**, *35*, 53; (b) Liu, Z.; Winnik, M. A.; Jao, T. C.; Rösch, J. *J. Phys. Chem. A* **1998**, *102*, 5349.
(26) Ohta, T.; Urakawa, O.; Tran-Cong, Q. *Macromolecules* **1998**, *31*, 6845.
(27) Zhou, C.; Winnik, M. A.; Jao, T. C. *J. Polym. Sci., A: Polym. Chem.* **2001**, *39*, 2642.
(28) Wu, C.; Xia, K. Q. *Rev. Sci. Instrum.* **1994**, *65*, 587.
(29) Kim, A. Y.; Berg, J. C. *Langmuir* **2000**, *16*, 2101.
(30) Zimm, B. H. *J. Chem. Phys.* **1948**, *16*, 1099.
(31) Berry, G. C. *J. Chem. Phys*. **1966**, *44*, 4550.
(32) Berne, B. J.; Pecora, R. *Dynamic Light Scattering*; Plenum Press: New York, 1976.
(33) Chu, B. *Laser Light Scattering*, 2nd ed.; Academic Press: New York, 1991.
(34) Stockmayer, W. H.; Schmidt, M. *Pure Appl. Chem*. **1982**, *5*4, 407.
(35) Biasio, A. D.; Bordi, F.; Cametti, C. *Colloids Surf. A* **1999**, *160*, 189.
(36) Kjøniksen, A.; Joabsson, F.; Thuresson, K.; Nyström, B. *J. Phys. Chem. B* **1999**, *103*, 9818.
(37) Sheludko, A. *Colloid chemistry*, Elsevier: New York, 1966; p 277.
(38) Vera, P.; Gallardo, V.; Salcedo, J.; Delgado, A. V. *J. Colloid Interface Sci.* **1996**, *177*, 553.
(39) Peck, D. G.; Johnston, K. P. *Macromolecules* **1993**, *26*, 1537.
(40) We use molar concentrations for particles and rate constants to facilitate comparison with reactions between molecules. Physicists prefer number densities. In these units, $k_{diff} = 6.2 \times 10^{-15}$ LS^{1-}.
(41) Lin, M. Y.; Lindsay, H. M.; Weitz, D. A.; Ball, R. C.; Klein, R.; Meakin, P. *Proc. R. Soc. London* **1989**, *A 423*, 71.
(42) Everett, D. H. *Basic Principles of Colloid Science*; Royal Society of Chemistry: London, 1988; p 34.
(43) Zhou, C.; Winnik, M. A.; Jao, T. C., manuscript in preparation.